UDC 539.4

Microstructure and Wear Resistance of an Arc-Sprayed Fe-Based Coating after Surface Remelting Treatment

H. L. Tian,[a,b,1] S. C. Wei,[b] Y. X. Chen,[b] H. Tong,[b] Y. Liu,[b] and B. S. Xu[b]

[a] School of Materials Science and Engineering, Beijing University of Aeronautics and Astronautics, Beijing, China

[b] National Key Laboratory for Remanufacturing, Academy of Armored Forces Engineering, Beijing, China

[1] haoliangtian@163.com

УДК 539.4

Микроструктура и износостойкость покрытия на основе железа, полученного электродуговой металлизацией, после обработки поверхности с помощью переплавки

Х. Л. Тиан[а,б,1], С. Ц. Вей[б], Й. К. Чен[б], Х. Тонг[б], Й. Лиу[б], Б. С. Ксу[б]

[а] Факультет материаловедения и машиностроения, Пекинский университет авиации и космонавтики, Пекин, Китай

[б] Национальная лаборатория модернизации, Инженерная академия бронетанковых войск, Пекин, Китай

Усовершенствованы пластинчатая структура и износостойкость покрытий, полученных электродуговой металлизацией. С помощью дуговой сварки вольфрамовым электродом в среде инертного газа проведена переплавка покрытий на основе FeNiCrAl, полученных электродуговой металлизацией. С использованием методов оптической микроскопии, растровой электронной микроскопии и дифракции рентгеновских лучей осуществлено сравнительное исследование структуры и фазового состава напыленных и переплавленных покрытий. Изучено влияние обработки путем переплавки на механизм износа покрытий, полученных электродуговой металлизацией. Установлено, что реализация дуговой сварки вольфрамовым электродом в среде инертного газа позволяет разрабатывать покрытия без пор и трещин. Дальнейшие исследования показали, что основной признак износа покрытий, полученных электродуговой металлизацией, – расщепление оксида, в то время как покрытий, переплавленных с помощью дуговой сварки вольфрамовым электродом в среде инертного газа, – резание и пропахивание.

Ключевые слова: высокоскоростная электродуговая металлизация, процесс переплавки, микроструктура, износ.

Introduction. The arc spraying process is widely used to prepare various thin coatings, and is especially applied in the maintaining and rebuilding fields [1]. However, the coatings obtained using this process exhibit lamellar microstructure, high porosity and low surface hardness and their wear resistance is not sufficient for many applications [2]. Therefore, a surface remelting treatment needs to be carried out to reinforce the adhesive strength and enhance the wear resistance of the as-sprayed coatings.

The reduction of microinclusion content of coatings by surface melting using processes such as laser [3], plasma [4] and tungsten inert gas (TIG) [5] welding has been shown to improve coating toughness owing to changes in microstructure, chemical composition and

oxygen content. In recent years, several studies have been performed using the TIG method [6]. The process increases surface hardness, improves wear resistance and results in little or no distortion. In this work, the microstructural properties, hardness, phase composition and wear resistance of Fe-based remelted coatings made using a TIG torch are reported.

Experimental Method. Fe–Ni–Cr–Al cored wire with a diameter of 2 mm was used to produce as-sprayed coatings. The chemical composition of the arc spraying wire was (wt.%): Ni < 10, Cr < 5, Al < 5, B < 1, Nb < 1, Re < 1, Fe – balance.

The wires were sprayed onto a grit blasted and degreased AISI 1045 steel substrate with dimensions of 100×100×10 mm using a self-designed HAS-02 wire arc gun system. The process parameters were optimized as follows: spraying voltage 28 V, spraying current 160 A, compressed air pressure 0.7 MPa, standoff distance, 200 mm. The thickness of the as-sprayed coatings was 400–500 μm and they were subsequently melted using a TIG torch. The TIG torch/arc was produced with an operating current ranging from 80 to 100 A. The remelting process was carried out at 3 and 4 mm/s speed and the electrode height from the substrate surface was varied between 3 and 5 mm. The shield gas flow (argon) was 12 l/min.

The microstructures and chemical compositions of cross sections of the as-sprayed and remelted samples were compared using optical microscopy, scanning electron microscopy (SEM) and energy dispersive spectroscopy (EDS). X-ray diffraction (XRD) analysis was conducted to determine the phases formed in the surface alloyed layer.

Dry sliding wear tests were carried out using a ball-on-plate reciprocating machine at room temperature (25°C). The counterpart ball was quenched before the wear test. The abrading ball was a GCr15 ball with 65 HRC and of 4 mm in diameter. The applied load and sliding distance were 50 N and 2700 mm (with an increment of 3 mm), respectively. The sliding velocity was 3 mm/s. Five samples were measured for each set of test parameters. The friction coefficient was monitored with a computer. The microstructures of worn surfaces and wear debris were analyzed by SEM to understand the wear mechanism for the coated and uncoated samples.

Results and Discussion.

X-Ray Diffraction. X-ray diffraction analysis was performed on the surface of the as-sprayed and remelted coatings. The diffraction patterns are shown in Fig. 1a and 1b, respectively. As can be seen from Fig. 1a, α-Fe, γ-Fe and Fe–Al intermetallic compounds are major phases present in the surface of the as-sprayed coating. Moreover, during spraying, molten liquid drops are exposed to air and are oxidized in flight to the substrate, and many oxides, such as Al_2O_3, Cr_2O_3, and Fe_3O_4, can be present at the exposed surfaces of splats prior to the deposition of the subsequent layer [7].

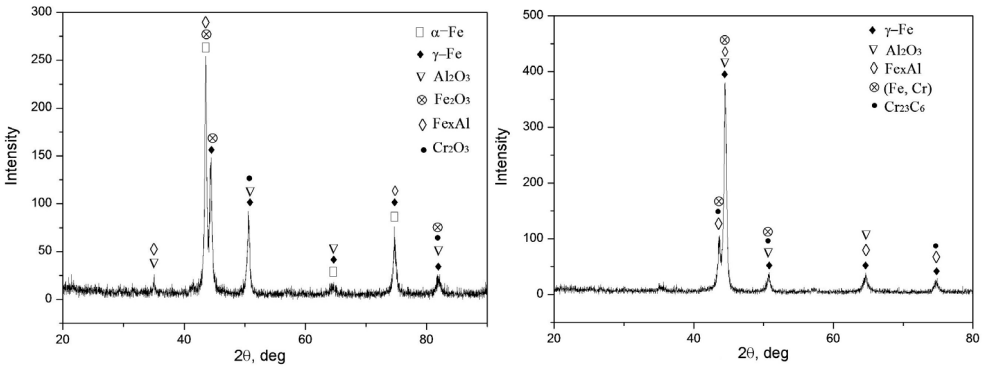

a b

Fig. 1. XRD results for as-sprayed (a) and remelted (b) coatings.

Figure 1b shows the phases of the remelted coating. These are mainly γ-Fe, Fe–Al intermetallic compounds, (Fe, Cr) solid solution and $Cr_{23}C_6$ carbides, and weak peaks are assigned to Al_2O_3 oxides. These results clearly confirm that the elements Fe, Cr, Ni, and Al dissolved in the coating matrix then formed more alloy phases, while few oxides were detected in the coating after the TIG remelting process.

Microstructural Examination. A comparison was made of the cross-sectional micrographs of the remelted coating formed by TIG (Fig. 2b) and the as-sprayed coating (Fig. 2a). A thin white layer is observed at the interface in Fig. 2b, which indicates a good metallurgical bonding between the remelted coating and the substrate.

At the bonding zone, an extremely high rate of heat transfer occurred between the molten pool and the substrate and a large melt was obtained under cooling leading to a very high rate of solidification [8]. The solid/liquid interface grew in a flat form giving rise to the formation of a bright flat grain in the coating as shown in Fig. 2b.

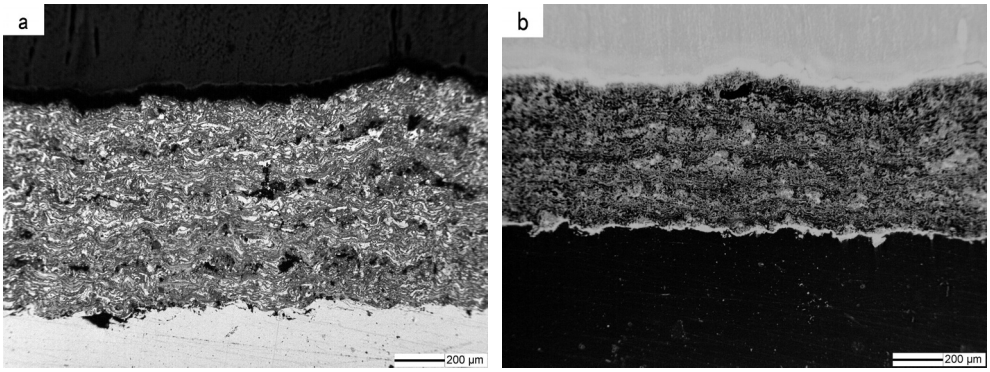

Fig. 2. Optical micrographs of cross sections of the as-sprayed (a) and the remelted (b) coatings.

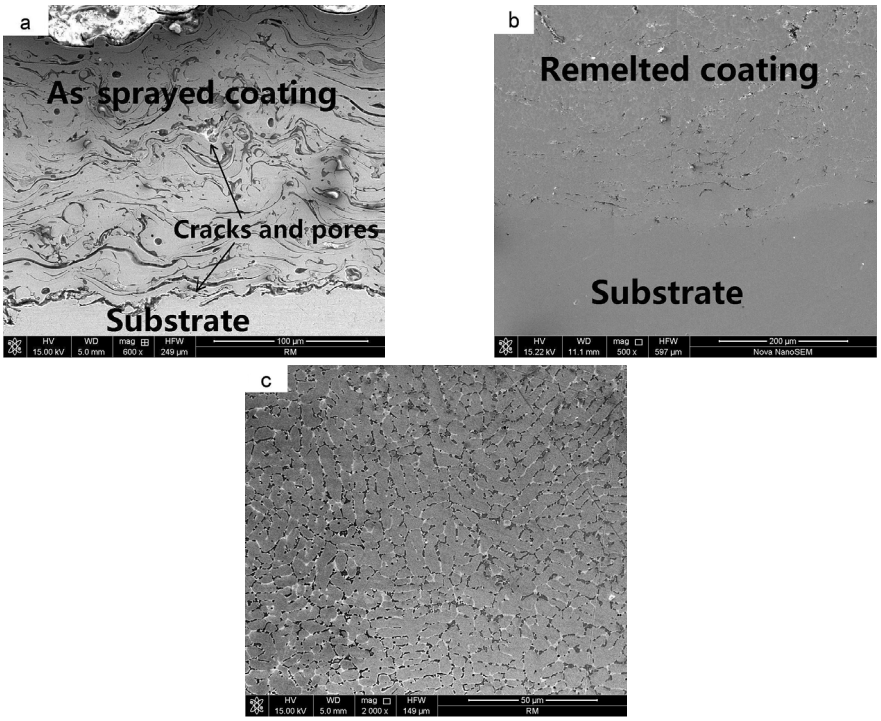

Fig. 3. SEM cross-sectional morphology of the as-sprayed (a) and the remelted (b) coatings and high magnification morphology (c).

Figure 3a shows a cross-sectional SEM image of the as-sprayed coating before TIG treatment. Laminated structures with many pores and cracks occur in the lamellar structure and the interface between the coating and substrate. Figure 3b shows the cross-sectional morphology of the remelted coating. In contrast to Fig. 3a, the remelted coating was characterized by a more homogeneous structure, absence of structure lamination, and decreased surface roughness and porosity. In order to analyze the porosities quantitatively, a computer image analyzer was employed. It was observed that the porosities of the as-sprayed coatings were 17–22% and the remelted coatings show a dramatically reduced porosity of only 1.1–2.8%.

A typical patter of higher magnification morphology observed for remelted coatings is shown in Fig. 3c. The SEM investigations revealed a distinct refinement of the structure. No microcracks delaminating the remelted coating were observed. Depending on the material cooling rate function of the adopted treatment parameters, different phase morphologies were observed of which microdendrite and cellular–dendrite were predominant.

Microhardness Investigations. The microhardness profiles of the as-sprayed and remelted coatings with coating depth are shown in Fig. 4. It can be seen that the microhardness of the as-sprayed coating gradually increased with increasing distance from the substrate to the coating surface. The hardness of the as-sprayed coating was about 480–580 HV0.1. The anisotropy of the coating, resulting from the characteristic layered structure of the as-sprayed material, was responsible for the microhardness values and their distributions.

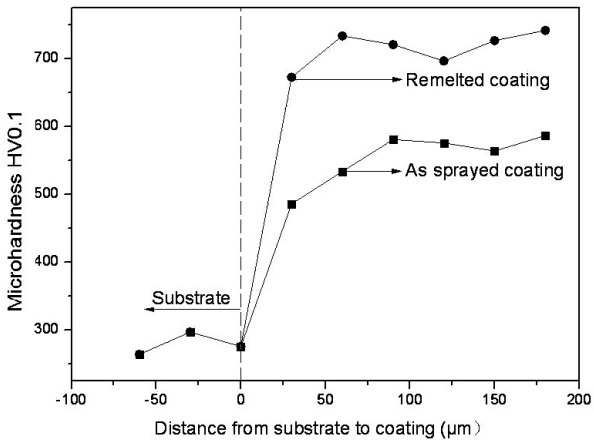

Fig. 4. Microhardness of the as-sprayed and remelted coatings.

The hardness increased to about 670–740 HV0.1 for the as-sprayed coating after remelting treatment. This result confirms that there are marked differences in the microstructures of the coatings before and after the TIG remelting process. The remelted coating exhibits a high hardness corresponding to hard phases such as intermetallic compounds and (Fe, Cr) solid solution distributed in the dense structure and homogeneous chemical dispersion as well as recrystallization.

Wear Resistance Performance. Comparing the substrate, as-sprayed coating and TIG remelted coating, the variations of friction coefficient are shown in Fig. 5. The average friction coefficient values of the substrate, as-sprayed coating and remelted coating were calculated as 0.9, 0.6, and 0.5, respectively. It can be seen that the TIG remelted coating is more effective in improving wear resistance, and its friction coefficient curve shows a smooth variation. Also, the friction coefficient curve of the remelted coating is more stable than that of the substrate with increasing sliding distance.

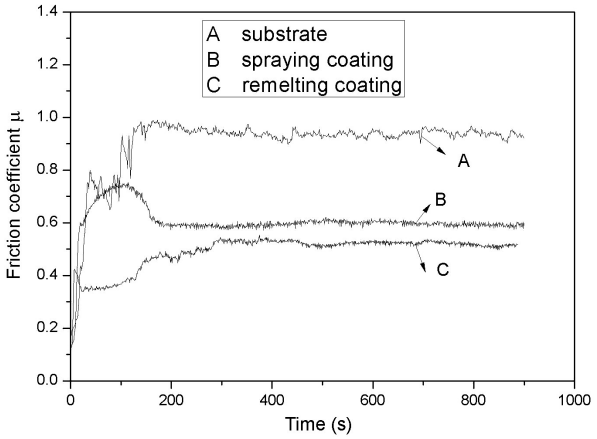

Fig. 5. Friction coefficients of the Fe-based coatings and substrate.

In order to compare the wear resistance of the as-sprayed coating and the remelted one, SEM examinations of the worn surfaces were undertaken, as shown in Fig. 6. It can be seen that the wear track of the remelted coating (Fig. 6c) is shallower than those of the as-sprayed coating (Fig. 6b) and the substrate (Fig. 6a). Also, the wear volume losses for the substrate, as-sprayed coating and remelted coating were measured as $3.78 \cdot 10^{-6}$, $2.46 \cdot 10^{-6}$, and $1.13 \cdot 10^{-6}$ μm^3, respectively, revealing that the TIG remelted coating has the lowest wear volume for the dense microstruture. A fine cellular structure was formed after the TIG remelting process.

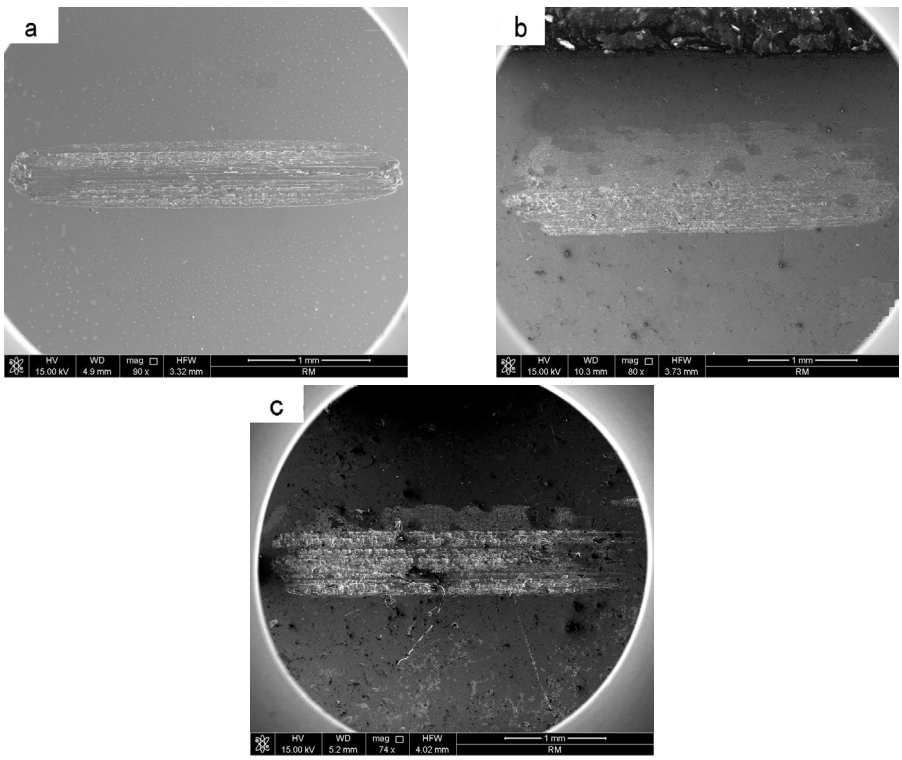

Fig. 6. Macrographics wear tracks of the substrate (a), the as-sprayed (b) and the remelted (c) coatings.

Aiming to understand the wear mechanisms of the as-sprayed and remelted coatings, SEM and EDS analyses of the wear surface and wear debris were undertaken, as shown in Figs. 7 and 8, respectively. The EDS examinations of the wear tracks of the as-sprayed coating confirmed that the chemical composition of the micro-zone of the wear surface is mainly 68.38 wt.% Fe, 9.28 wt.% Al, 21.13 wt.% O, and 1.21 wt.% Nb (Fig. 7b). The results show the presence of iron oxides on practically all the surfaces of the coatings that were tested (Fig. 7a). The concentration of these oxides fell as the sliding distance increased. This can be explained by the low cohesive strength among splats, numerous pores and microcracks already present in the as-sprayed coating or generated during the tests carried out. Under the dry sliding conditions, the induced strong shearing stress initiates microcracks, which, together with inherent microcracks, grow and extend along the boundaries of the splats. When the stress intensity is close to the fracture toughness of the coating, complete splats should break off from the coating [9].

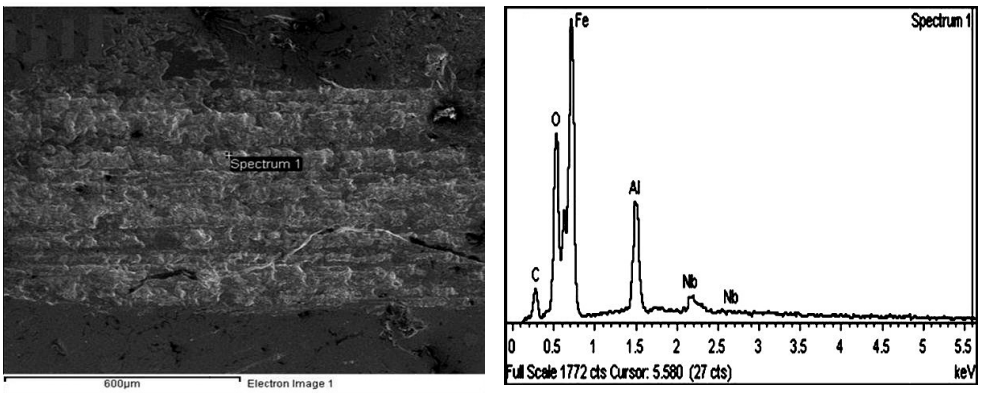

a b

Fig. 7. SEM and EDS analyzes of the as-sprayed coating: (a) SEM morphology of the wear track; (b) EDS analysis of the wear track.

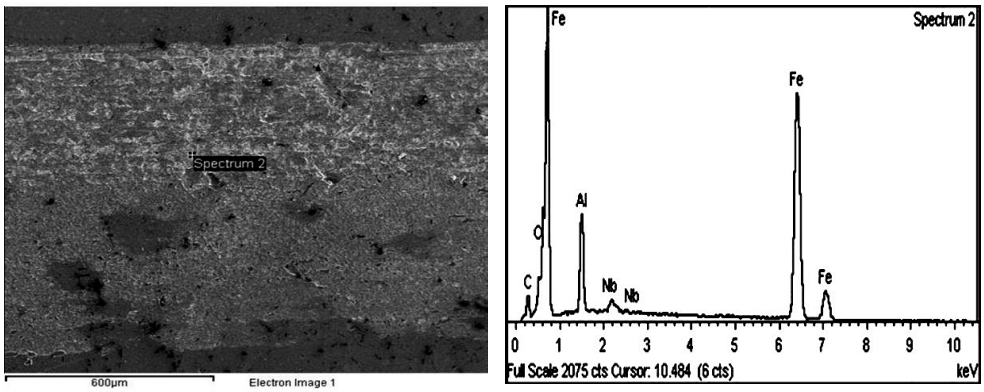

a b

Fig. 8. SEM and EDS analyzes of the remelted coating: (a) SEM morphology of the wear track; (b) EDS analysis of the wear track.

The wear surface of the remelted coating is distinguished by discontinuous parallel grooves (see mark-up spectrum *2* in Fig. 8a), which form as the hard abrasive phases dig into the worn coating surface and then plough out the matrix material from the groove to the side. This causes the so-called grooving wear mode [10]. Therefore, cutting and ploughing are the main abrasive wear mechanisms. But, the distribution of the (Fe, Cr)

solid solution and $Cr_{23}C_6$ hard phases surrounded by a matrix of γ-Fe will be of benefit for improving the wear resistance. The surrounding ductile structure (γ-Fe) will absorb energy, while the coating bears a high load, releasing the residual stress [11]. This structural characteristic of abrasive particles embedded in the ductile matrix will prevent the microcracks often initiated from inside of the oxide boundaries with the action of concentrated stresses and improve the wear resistance of the remelted coating. Furthermore, oxygen atoms were not detected in the wear surface (Fig. 8b), which confirms that the remelted coating has the ability to resist oxidation wear failure. The very dense microstructure and low porosity characteristics also prevent the abrasive particles from microcutting the surface by breaking them up and causing them to lose their cutting function [12]. Therefore, the coating has excellent abrasive wear resistance.

Conclusions

1. Coatings produced by TIG remelting of Fe-based alloy coatings are free from pores and cracks and show good metallurgical bonding with the substrate. The primary phases of the remelted coating were identified as $Cr_{23}C_6$ carbides and Fe-based solid solution.

2. The consequence of the remelting treatment is the transformation α-Fe $\rightarrow \gamma$-Fe. The wear resistance of coated samples is far better than that of uncoated samples. Particles of thin flake sheet form combined with the energy dispersive spectroscopic analysis confirm that oxide delamination is the dominant wear mechanism of the as-sprayed coating. Cutting and ploughing are the main abrasive wear mechanisms of the remelted coating.

Acknowledgements. The authors are grateful for the support provided by 973 Project (2011CB013403), and the Natural Science Foundation of China (51105377, 50971132), National Science and Technology Supporting Project (No. 2011baf11B07).

Резюме

Удосконалено пластинчасту структуру та зносостійкість покриттів, отриманих електродуговою металізацією. За допомогою дугового зварювання вольфрамовим електродом у середовищі інертного газу проведено переплавку покриттів на основі FeNiCrAl, отриманих електродуговою металізацією. Із використанням методів оптичної мікроскопії, растрової електронної мікроскопії та дифракції рентгенівських променів проведено порівняльне дослідження структури і фазового складу напилених і переплавлених покриттів. Вивчено вплив обробки шляхом переплавки на механізм зношення покриттів, отриманих електродуговою металізацією. Установлено, що реалізація дугового зварювання вольфрамовим електродом у середовищі інертного газу дозволяє розробляти покриття без пор і тріщин. Подальші дослідження показали, що основними ознаками зношення покриттів, отриманих електродуговою металізацією, є розщеплення оксиду, в той час як покриттів, переплавлених за допомогою дугового зварювання вольфрамовим електродом у середовищі інертного газу, – різання і проорювання.

1. Y. X. Chen, X. B. Liang, Y. Liu, et al., “Effect of heat treatment on microstructure and residual stress of wire arc sprayed high carbon steel coating,” *Surf. Eng.*, **26**, 407–412 (2010).
2. S. Buytoz and M. Ulutan, “In situ synthesis of SiC reinforced MMC surface on AISI 304 stainless steel by TIG surface alloying,” *Surf. Coat. Technol.*, **200**, 3698–3704 (2006).
3. N. Ahmed, M. S. Bakare, D. G. McCartney, and K. T. Voisey, “The effects of microstructural features on the performance gap in corrosion resistance between bulk and HVOF sprayed Inconel 625,” *Surf. Coat. Technol*., **204**, 2294–2301 (2010).

4. T. T. Wong, G. Y. Liang, G. An, and J. M. K. MacAlpine, "The electrical conductivity of laser-remelted and plasma-sprayed Ni and Cr coatings," *J. Mater. Process. Technol*., **159**, 265–271 (2005).
5. B. Arivazhagan, S. Sundaresan, and M. Kamaraj, "Effect of TIG arc surface melting process on weld metal toughness of modified 9Cr–1Mo (P91) steel," *Mater. Lett.*, **62**, 2817–2820 (2008).
6. Y. Shi, H. Zhang, and S. Y. Liu, "Laser fine cladding on miniature thin wall parts," *Surf. Eng*., **27**, 464–469 (2011).
7. J. Morimoto, Y. Sasaki, and S. Fukuhara, "Surface modification of Cr_3C_2–NiCr cermet coatings by direct diode laser," *Vacuum*, **80**, 1400–1405 (2006).
8. G. Azimi and M. Shamanian, "Effects of silicon content on the microstructure and corrosion behavior of Fe–Cr–C hardfacing alloys," *J. Alloys Compd.*, **505**, 598–603 (2010).
9. Y. X. Chen, B. S. Xu, and Y. Liu, "Structure and sliding wear behavior of 321 stainless steel/Al composite coating deposited by high velocity arc spraying technique," *Trans. Nonferrous Met. Soc. China*, **18**, 603–609 (2008).
10. J. B. Cheng, X. B. Liang, and B. S. Xu, "Formation and properties of Fe-based amorphous/nanocrystalline alloy coating prepared by wire arc spraying process," *J. Non-Cryst. Solids*, **355**, 1673–1678 (2009).
11. M. Vite, M. Castillo, and L. H. Hernandez, "Dry and wet abrasive resistance of Inconel 60 and stellite," *Wear*, **258**, 70–76 (2005).
12. J. M. Miguel, J. M. Guilemany, and S. Vizcaino, "Tribological study of NiCrBSi coating obtained by different processes," *Tribol. Int.*, **36**, 181–187 (2003).

Received 22. 11. 2013